Supporting Information:

Full-Dimensional Theory of Pair-Correlated HNCO Photofragmentation

L. Bonnet,[*,†] R. Linguerri,[‡] M. Hochlaf,[*,‡] O. Yazidi,[¶] P. Halvick,[†] and J. S. Francisco[§]

Institut des Sciences Moléculaires, Université de Bordeaux, CNRS, UMR 5255, 33405, Talence, France, Laboratoire Modélisation et Simulation Multi Echelle, Université Paris-Est, UMR 8208 CNRS, 5 Bd Descartes, 77454 Marne La Vallée, France, Laboratoire de Spectroscopie Atomique, Moléculaire et Applications, LR01ES09, Faculté des Sciences de Tunis, Université de Tunis El Manar, 2092 Tunis, Tunisia, and Department of Chemistry, University of Nebraska-Lincoln, 433 Hamilton Hall, Lincoln, Nebraska 68588-0304, USA

E-mail: claude-laurent.bonnet@u-bordeaux.fr; hochlaf@univ-mlv.fr

[*]To whom correspondence should be addressed

[†]Institut des Sciences Moléculaires, Université de Bordeaux, CNRS, UMR 5255, 33405, Talence, France

[‡]Laboratoire Modélisation et Simulation Multi Echelle, Université Paris-Est, UMR 8208 CNRS, 5 Bd Descartes, 77454 Marne La Vallée, France

[¶]Laboratoire de Spectroscopie Atomique, Moléculaire et Applications, LR01ES09, Faculté des Sciences de Tunis, Université de Tunis El Manar, 2092 Tunis, Tunisia

[§]Department of Chemistry, University of Nebraska-Lincoln, 433 Hamilton Hall, Lincoln, Nebraska 68588-0304, USA

We detail here the construction of the 6D-PES and the dynamical calculations of kinetic energy distributions (KEDs), rotational energy distributions (REDs), vibrational state populations (VSDs) and anisotropy parameters (APs). Fig. X and Fig. SX refer to the X^{th} figures of the letter and the present document, respectively.

Potential energy surface

The S_1 PES by Klossika and Schinke (KS)[1] is a five-dimensional function corresponding to all atoms confined to a plane. This function was fitted to *ab-initio* calculations, performed using the multi-reference configuration-interaction method with triple-zeta basis set. The KS-PES depends on the five coordinates $(r_{HN}, r_{NC}, r_{CO}, \alpha, \beta)$ represented in Fig. 1. The dyhedral or torsion angle γ is chosen equal to π for the *trans* configuration displayed in this figure. The rationale for constraining the five atoms to a plane is that for any fixed values of the previous coordinates in the strong coupling region, the dependence of the potential energy on γ involves two minima at γ equal 0 and π, i.e., for planar geometries. Moreover, the equilibrium geometry in the electronic ground state S_0 is also planar. Consequently, if the system is optically excited from the equilibrium geometry of S_0 with the nuclei at rest, up to the excited state S_1, it is expected to keep planar throughout the whole fragmentation. This is, however, a classical picture neglecting the zero point energy (ZPE) along the γ coordinate. Quantum mechanically, out-of-plane motions cannot be frozen, and these can possibly be amplified during the dissociation.

With the aim of improving the realism of our simulations, we have thus deduced a six-dimensional function from the KS-PES which now depends on γ and is expected to semi-quantitatively account for the previous out-of-plane motions. This extension is based on the following reasoning: it is clear from Fig. 4 of ref. 1 that immediately after the photon absorption, strong torques are expected to quickly drive the system from the equilibrium geometry of S_0, for which $\alpha \approx 172^\circ$, towards the *trans* or *cis* minima of S_1, for which $\alpha \approx 125.4^\circ$ and 231°, respectively, with a concomitent increase of r_{NC}. In a second step corresponding to barrier crossing at a more moderate

speed, α is expected to oscillate around the previous values over a large portion of the dissociation path. Fig. 6 of ref. 1 suggests that β should roughly behave as α. It thus makes sense to approximate the full-dimensional PES by the sum of (i) the KS-PES and (ii) a term depending mainly on γ and r_{NC} fitted to *ab-initio* calculations (see further below) with the rest of the coordinates kept at the values of the *trans* or *cis* minima. This term must be equal to 0 for γ equal 0 and π, so the full-dimensional PES matches the KS-PES for planar configurations. These requirements are fulfilled by the following expression:

$$V(\mathbf{r},\gamma) = S(\gamma)V_0(\mathbf{r},\gamma) + [1 - S(\gamma)]\,V_\pi(\mathbf{r},\gamma) \tag{1}$$

with

$$V_0(\mathbf{r},\gamma) = V_0^{KS}(\mathbf{r}) + V_0^{Torsion}(\gamma, r_{NC})\,(sin\alpha sin\beta)^{\frac{1}{4}}\,, \tag{2}$$

$$V_\pi(\mathbf{r},\gamma) = V_\pi^{KS}(\mathbf{r}) + V_\pi^{Torsion}(\gamma, r_{NC})\,(sin\alpha sin\beta)^{\frac{1}{4}}\,, \tag{3}$$

$$V_0^{Torsion}(\gamma, r_{NC}) = V^{Torsion}(\gamma, r_{NC}) - V^{Torsion}(0, r_{NC}), \tag{4}$$

$$V_\pi^{Torsion}(\gamma, r_{NC}) = V^{Torsion}(\gamma, r_{NC}) - V^{Torsion}(\pi, r_{NC}) \tag{5}$$

and

$$S(\gamma) = \frac{e^{-\delta(\gamma-\pi/2)}}{e^{\delta(\gamma-\pi/2)} + e^{-\delta(\gamma-\pi/2)}}. \tag{6}$$

$\mathbf{r}$ is vector $(r_{HN}, r_{NC}, r_{CO}, \alpha, \beta)$. $V_\pi^{KS}(\mathbf{r})$ is the KS-PES. In ref. 1, α and β both belong to the range $[0, 2\pi]$. However, introducing γ now limits α and β to the range $[0, \pi]$. $V_\pi^{KS}(\mathbf{r})$ is thus the KS-PES for the *trans* configuration (γ equal π). $V_0^{KS}(\mathbf{r})$, the KS-PES for the *cis* configuration (γ equal 0), is deduced from $V_\pi^{KS}(\mathbf{r})$ by

$$V_0^{KS}(\mathbf{r}) = V_\pi^{KS}(\bar{\mathbf{r}}) \tag{7}$$

where $\bar{\mathbf{r}}$ is vector $(r_{HN}, r_{NC}, r_{CO}, \alpha, 2\pi - \beta)$. $V^{Torsion}(\gamma, r_{NC})$ is the torsional term depending on γ and r_{NC} fitted to *ab-initio* calculations (see further below) with r_{HN}, r_{CO}, α and β kept at the values corresponding to the *trans* or *cis* minima (in the $(r_{HN}, r_{NC}, r_{CO}, \alpha, \beta, \gamma)$ space)). These

values are not the same for the two minima, but are very close. For simplicity's sake, we have thus taken the average of both sets of values. $V_0(\mathbf{r},\gamma)$ and $V_\pi(\mathbf{r},\gamma)$ are the six-dimensional extensions of the KS-PES in the neighborhood of the *trans* and *cis* planar geometries, respectively. The factor $(sin\alpha sin\beta)^{\frac{1}{4}}$ has been introduced in order to cancel the torsional contribution to the potential whenever α or β take the value 0. The power one fourth makes the previous factor close to one for any value of α or β not too close to 0 and π. Finally, $S(\gamma)$ is a switching function ensuring a smooth transition between $V_0(\mathbf{r},\gamma)$ and $V_\pi(\mathbf{r},\gamma)$ around γ equal $\pi/2$.

For the calculation of the $V^{Torsion}(\gamma, r_{NC})$ term in Eqs. (4) and (5), we employed the equation-of-motion coupled-cluster approach[2] (EOM-CC) applied to the coupled-cluster singles and doubles[3] (CCSD) model, where excited state energies have been obtained by solving the EOM-CC right eigenvalue equations. The atomic basis set adopted in this study is the aug-cc-pVTZ set of Dunning and co-workers.[4,5] These computations have been carried out with the MOLPRO[6] (2012.1 version) package of *ab-initio* programs. For the S_1 state, the EOM-CC energies should be accurate within 0.1-0.3 eV (in absolute values).

Dynamical calculations

The dynamical calculations were performed by means of a homemade code. The rotational angular momentum of HNCO was assumed to be 0, as is mostly the case in the experiment of Yang and co-workers.[7,8] In a first step, we determined the transformation from normal mode to Cartesian coordinates around the equilibrium geometry of HNCO in S_0, previously stated to be planar. The Cartesian coordinates (x,y,z) are kept along the principle axes of inertia of HNCO in the previous geometry (see Fig. 1). x and y are chosen to lie within the HNCO plane. z is thus orthogonal to this plane. (x,y,z) is a body-fixed frame. The state of HNCO before the optical excitation, i.e., the vibrational ground state in S_0, was expressed as a product of six Gaussian functions, each depending on one of the normal mode coordinates. The Wigner distribution associated with the previous state turns out to be a product of twelve Gaussians, each depending on one of the normal mode

coordinates or their conjugate momenta.[9] Following Goursaud *et al.*,[10] the initial normal mode coordinates and momenta were selected by importance sampling according to the previous Wigner distribution (see also ref. 9). The transformation from normal mode to Cartesian coordinates was used to generate the 12 Cartesian coordinates of the four atoms as well as their 12 conjugate momenta. These 24 phase space coordinates served as initial conditions of the trajectories that were run by using the 4th-order Runge-Kutta integrator[11] on the modified KS-PES (see Eqs. (1)-(7)) until they reached the products. In practice, trajectories were stopped at $r_{NC} = 8.5$ bohr, where ^{1}NH and CO no longer interact. From the final conditions, we calculated the following trajectory outcomes: (i) the kinetic or translational energy E_T, (ii) the vibrational actions a_{NH} and a_{CO} of the free diatom ^{1}NH and CO (see Appendix A in ref. 12), (iii) their rotational angular momenta J_{NH} and J_{CO} in $\hbar$ unit and (iv) the modulous v of the relative velocity vector and its projection v_z on the z-axis. We show in the three next subsections how the KEDs, VSPs and APs are deduced from the previous quantities. In the next developments, $nint(x)$ and $int(x)$ are, respectively, the nearest integer and real part of x.

Kinetic energy distributions

CO as co-product

We first focus on the case where the co-product is CO.[8] The pair-correlated KED, called $P(E_T)$ in the following, is measured for ^{1}NH in quantum state (n_{NH}, j_{NH}). Call N the total number of trajectories run. We consider the same range [0, 9000 cm^{-1}] as Zhang *et al.*[8] (see Fig. 4), and divide it in 100 bins 90 cm^{-1} wide (this number is of course arbitrary). The discretized form of $P(E_T)$ is then given by the probabilities P^i that E_T belongs to the range $[90(i-1), 90i]$, $i = 1-100$, the final quantum state of ^{1}NH being (n_{NH}, j_{NH}). Within GB-CTM, these probabilities read

$$P^i \propto \sum_{k=1}^{N} G_\varepsilon(a_{NH}^k - n_{NH})\, B_{j_{NH}}^k\, B_{KE}^{ik} \sum_{n_{CO}=0}^{n_{CO}^{max}} G_\varepsilon(a_{CO}^k - n_{CO}). \tag{8}$$

The left-hand sum is over the whole set of trajectories. The right-hand sum is over the available vibrational states of CO. Calling J_{NH}^k the value of J_{NH} for the k^{th} trajectory, $B_{j_{NH}}^k$ is a Boolean variable equal to one if J_{NH}^k belongs to the range $[j_{NH}, j_{NH}+1]$, zero otherwise. B_{KE}^{ik} is also a Boolean variable equal to one if the kinetic energy E_T^k for the k^{th} trajectory lies within the i^{th} bin, zero in the contrary case. Setting

$$G_\varepsilon(x) = \frac{1}{\pi^{1/2}\varepsilon} exp\left[-\left(\frac{x}{\varepsilon}\right)^2\right], \tag{9}$$

$G_\varepsilon(a_{NH}^k - n_{NH})$ and $G_\varepsilon(a_{CO}^k - n_{CO})$ are Gaussian weights[12] ensuring Bohr's condition of vibrational quantization of ^{1}NH and CO. a_{NH}^k and a_{CO}^k are the values of a_{NH} and a_{CO} for the k^{th} trajectory. These weights are normalized to unity (integrating $G_\varepsilon(x)$ over x leads to 1). The full-width-at-half-maximum (FWHM) of Gaussian weights is equal to $2\,(ln2)^{1/2}\,\varepsilon$. As previously stated, Bohr's condition of quantization assigns an infinite statistical weight to those classical trajectories reaching the products with integer values of both a_{NH} and a_{CO}, while this weight is zero for the remaining paths. In other words, a strict application of Bohr quantization rule would require keeping ε at 0, thereby making the right-hand sum of Eq. (8) a Dirac comb. This would, however, render the calculations unfeasible, since the set of trajectories leading to integer actions is of zero measure. Generally, ε is kept at 0.06, corresponding to a FWHM of 10 %, a reasonably small value as compared to the unit spacing between two neighbouring Gaussians in the comb. Since Gaussians do not overlap, Eq. (8) can be simplified to

$$P^i \propto \sum_{k=1}^{N} G_\varepsilon(a_{NH}^k - n_{NH})\; G_\varepsilon(a_{CO}^k - nint\left(a_{CO}^k\right))\; B_{j_{NH}}^k\; B_{KE}^{ik}. \tag{10}$$

At this point, a comment on the experimental measurement of $P(E_T)$ is in order. Call E the total energy available to the final products ^{1}NH and CO. In an ideal experiment where perfect control of both E and the measurement of E_T would be achieved, E_T, equal to E minus the quantized internal energy of the products, would also be quantized. Consequently, $P(E_T)$ would be given by a set of Dirac peaks with given weights. In our calculations, however, we pseudo-quantize the vibrational

motions of ^{1}NH and CO through the GB procedure, but not their rotational motions. $P(E_T)$ is thus a rough approximation of what would be observed if inaccuracies in the measurements would introduce a blurring of the peaks slightly exceeding the average spacing between them. In reality, however, the blurring is much larger, for reagent states, beam collimation, etc, are not fully controlled and VMI itself significantly contributes to the blurring. We thus take this into account in the calculation of KEDs through the Gaussian convolution

$$P_c(E_T) = \int dE'_T \; G_\eta(E'_T - E_T) \; P(E'_T). \tag{11}$$

The discretized form of $P_c(E_T)$, thus, reads

$$P_c^i \propto \sum_{k=1}^{N} G_\varepsilon(a_{NH}^k - n_{NH}) \; G_\varepsilon(a_{CO}^k - nint\left(a_{CO}^k\right)) \; B_{j_{NH}}^k \sum_{j=1}^{100} B_{KE}^{jk} \; G_\eta(90(j-i)). \tag{12}$$

The value of η is chosen so as to reproduce as satisfyingly as possible the experimental KEDs at the threshold and cut-off. The theoretical KEDs in Fig. 4 have been calculated from Eq. (12).

^{1}NH as co-product

The ^{1}NH co-product case[7] involves developments similar to the previous ones, but requires an additional quantum constraint in order to reproduce the experimentally observed rotational resolution (see right-panels in Fig. 3). In an ideal experiment where perfect energy resolution would be achieved, the dashed curves in the previous panels would reduce to Dirac peaks, located at values of E_T corresponding to the teeth of the combs displayed in Fig. 3. In our GB-CTM calculations, however, rotational motions are classically treated, thus implying that E_T is not quantized. Nevertheless, the quantum value E_T^{QM} of the kinetic energy to which a given trajectory is expected to contribute can be straightforwardly deduced from the trajectory outcomes E_T, a_{NH}, a_{CO}, J_{NH} and J_{CO}. The deduction is as follows: the trajectory leading to a_{NH}, a_{CO}, J_{NH} and J_{CO} is supposed to contribute to the quantum state ($nint(a_{NH})$, $nint(a_{CO})$, $int(J_{NH})$, $int(J_{CO})$) with the Gaussian weight $G_\varepsilon(a_{NH} - nint(a_{NH})) \; G_\varepsilon(a_{CO} - nint(a_{CO}))$. Within the rigid rotor harmonic oscillator

(RRHO) approximation, the quantum value E_T^{QM} of the kinetic energy consistent with the previous state satisfies the identity

$$E = E_T^{QM} + E_{NH}^{QM} + E_{CO}^{QM} \tag{13}$$

with

$$E_{NH}^{QM} = \hbar\omega_{NH}\left[nint\left(a_{NH}\right) + \frac{1}{2}\right] + \frac{\hbar^2 int\left(J_{NH}\right)\left[int\left(J_{NH}\right)+1\right]}{2m_{NH}{r_{NH}^e}^2} \tag{14}$$

and

$$E_{CO}^{QM} = \hbar\omega_{CO}\left[nint\left(a_{CO}\right) + \frac{1}{2}\right] + \frac{\hbar^2 int\left(J_{CO}\right)\left[int\left(J_{CO}\right)+1\right]}{2m_{CO}{r_{CO}^e}^2}. \tag{15}$$

ω_{NH} and ω_{CO} are the vibrational frequencies of ^{1}NH and CO, m_{NH} and m_{CO} are their reduced masses and r_{NH}^e and r_{CO}^e are their equilibrium bond lengths. Besides, the classical value E_T satisfies (still within the RRHO approximation)

$$E = E_T + E_{NH}^{CM} + E_{CO}^{CM} \tag{16}$$

with

$$E_{NH}^{CM} = \hbar\omega_{NH}\left(a_{NH} + \frac{1}{2}\right) + \frac{\hbar^2 J_{NH}^2}{2m_{NH}{r_{NH}^e}^2} \tag{17}$$

and

$$E_{CO}^{CM} = \hbar\omega_{CO}\left(a_{CO} + \frac{1}{2}\right) + \frac{\hbar^2 J_{CO}^2}{2m_{CO}{r_{CO}^e}^2}. \tag{18}$$

From Eqs. (13) and (16), we thus arrive at

$$E_T^{QM} = E_T + E_{NH}^{CM} - E_{NH}^{QM} + E_{CO}^{CM} - E_{CO}^{QM}. \tag{19}$$

Eqs. (14), (15), (17)-(19) are the expected relations giving the dependence of E_T^{QM} on E_T, a_{NH}, a_{CO}, J_{NH} and J_{CO}. Since Eq. (19) is only approximate, we have found that for a given state ($nint(a_{NH})$, $nint(a_{CO})$, $int(J_{NH})$, $int(J_{CO})$), the value of E_T^{QM} fluctuates around the unique value that it should in principle take. However, the range of fluctuation is sufficiently narrow to make the uncertainty on E_T^{QM} reasonably small. In other words, our method slightly thicken the teeths of the

combs displayed in Fig. 3 without making them overlap. One notes, however, that the difference $E_{NH}^{CM} - E_{NH}^{QM} + E_{CO}^{CM} - E_{CO}^{QM}$ between the quantum and classical internal energies of ^{1}NH and CO could be rigorously calculated using the exact values of the quantum and classical internal energies of the final diatom. This would allow to recover the combs in Fig. 3. In the present case, however, we have not found it necessary to follow this approach owing to the good quality of our predictions.

We now wish to calculate the KEDs measured for ^{1}NH and CO in the quantum states (n_{NH}, j_{NH}) and (n_{CO}, j_{CO}) (see dashed curves in Fig. 3). These KEDs are obtained by repeating the same type of calculations as in the previous part, but with E_T^{QM} instead of E_T. We thus consider the same range [0, 4000 cm^{-1}] as Wang *et al.*[7] (see Fig. 3), and divide it in 100 bins 40 cm^{-1} wide. The GB-CTM probabilities P^i that E_T^{QM} belongs to the range $[40(i-1), 40i]$, $i = 1-100$, the final quantum states of ^{1}NH and CO being (n_{NH}, j_{NH}) and (n_{CO}, j_{CO}), are given by

$$P^i \propto \sum_{k=1}^{N} G_\varepsilon(a_{NH}^k - n_{NH})\, B_{j_{NH}}^k\, G_\varepsilon(a_{CO}^k - n_{CO})\, B_{j_{CO}}^k\, B_{KE}^{ik}. \tag{20}$$

The definition of the Boolean terms is the same as in Eq. (8), the only difference being that E_T^{QM} is substituted to E_T in the calculation of B_{KE}^{ik}. After convolution, we finally arrive at

$$P_c^i \propto \sum_{k=1}^{N} G_\varepsilon(a_{NH}^k - n_{NH})\, B_{j_{NH}}^k\, G_\varepsilon(a_{CO}^k - n_{CO})\, B_{j_{CO}}^k \sum_{j=1}^{100} B_{KE}^{jk}\, G_\eta(40(j-i)). \tag{21}$$

The theoretical dashed KEDs in Fig. 3 have been calculated from Eq. (21). The theoretical solid curve was obtained by summing the previous ones (sum over j_{NH}). The codes used for these calculations are available on demand.

Rotational energy distributions

Within the RRHO approximation, the distribution of the rotational energy of CO is given by

$$P^i \propto \sum_{k=1}^{N} G_\varepsilon(a_{CO}^k - nint\left(a_{CO}^k\right))\, G_\varepsilon(a_{NH}^k - nint\left(a_{NH}^k\right))\, B_{RE}^{ik}. \tag{22}$$

B^{ik}_{RE} is equal to one if the CO rotational energy (right-most term in Eq. (15)) for the k^{th} trajectory lies within the i^{th} previously defined bin (see paragraph before Eq. (8)), zero in the contrary case. The distribution of the rotational energy of ^{1}NH is analogously calculated.

Vibrational state distributions

The population of the n_{CO} state correlated with (n_{NH}, j_{NH}) is given by

$$P_{n_{CO}} = \frac{\sum_{k=1}^{N} G_\varepsilon(a^k_{NH} - n_{NH}) B^k_{j_{NH}} G_\varepsilon(a^k_{CO} - n_{CO})}{\sum_{k=1}^{N} G_\varepsilon(a^k_{NH} - n_{NH}) B^k_{j_{NH}} G_\varepsilon(a^k_{CO} - nint\left(a^k_{CO}\right))}. \tag{23}$$

In order to avoid heavy notations, n_{NH} and j_{NH} do not explicitely appear as subscripts or upper-scripts in $P_{n_{CO}}$. The population of the n_{NH} state correlated with (n_{CO}, j_{CO}) is given by an analogous expression. The latter is useless here, however, since only the vibrational ground state of ^{1}NH is available in the experiment of Wang *et al.*[7]

Anisotropy parameters

The anisotropy parameter $\beta_{n_{CO}}$ measured by Zhang *et al.*[8] is given by[13]

$$\beta_{n_{CO}} = 2 < P_2(cos\theta_{v\mu}) > . \tag{24}$$

P_2 is the second Legendre polynomial, $\theta_{v\mu}$ is the angle between the velocity vector **v** and the transition dipole moment $\boldsymbol{\mu}$ in the body-fixed frame (x, y, z), and the average is over the trajectories contributing to state n_{CO}. As previously outlined, the equilibrium geometry in S_0 is planar. Before the optical excitation, the system is in the vibrational ground state, thus implying that the amplitude of the vibrational motions around the equilibrium geometry is small. In particular, out-of-plane motions are reduced. We thus neglect them and assume that HNCO is planar. Within this reasonable approximation, *ab-initio* calculations show that $\boldsymbol{\mu}$ for the $S_1 \leftarrow S_0$ transition is perpendicular to the HNCO plane. In other words, this moment is parallel to the z-axis. We thus

have

$$cos\theta_{v\mu} = \frac{v_z}{v}. \tag{25}$$

From Eqs. (24) and (25), the GB-CTM expression of $\beta_{n_{CO}}$ reads

$$\beta_{n_{CO}} = \frac{2\sum_{k=1}^{N} G_\varepsilon(a_{NH}^k - n_{NH}) B_{j_{NH}}^k G_\varepsilon(a_{CO}^k - n_{CO}) P_2(v_z^k/v^k)}{\sum_{k=1}^{N} G_\varepsilon(a_{NH}^k - n_{NH}) B_{j_{NH}}^k G_\varepsilon(a_{CO}^k - n_{CO})}. \tag{26}$$

Again, n_{NH} and j_{NH} do not explicitely appear as subscripts or upperscripts in $\beta_{n_{CO}}$ so as to avoid heavy notations.

Analogously, the anisotropy parameter $\beta_{j_{NH}}$ measured by Wang *et al.*[7] for $n_{NH} = 0$ is given by

$$\beta_{j_{NH}} = \frac{2\sum_{k=1}^{N} G_\varepsilon(a_{NH}^k) B_{j_{NH}}^k G_\varepsilon(a_{CO}^k - n_{CO}) B_{j_{CO}}^k P_2(v_z^k/v^k)}{\sum_{k=1}^{N} G_\varepsilon(a_{NH}^k) B_{j_{NH}}^k G_\varepsilon(a_{CO}^k - n_{CO}) B_{j_{CO}}^k}. \tag{27}$$

Trajectory calculations of APs for polyatomic fragmentations can also be found in refs. 14 and 15.

Additional results

The distributions of the rotational energies of ^{1}NH and CO at 210 and 201 nm are displayed in Fig. S1. Additional results regarding the KEDs measured in the experiment at 201 nm are provided in Figs. S2-S4. The GB-CTM VSDs and APs are shown in Fig. S5, to be compared with Fig. 3 in ref. 8. The distribution of the dihedral angle γ at the TS is represented in Fig. S6.

As previously outlined, theory tends to underestimate APs somehow. One may wonder whether internal conversion towards the electronic ground state S_0, which is ignored in our simulation, could not improve the predictions. For those trajectories hopping on S_0, the lifetime of HNCO would indeed be much larger, for trajectories would be trapped within a much deeper well than in S_1. Therefore, the anisotropy parameter for these hopping trajectories would be close to 0, thus making the overall APs larger than $\sim$ -0.9, and hence, in better agreement with experiment. Another reason why our APs are lower than the experimental ones might be that $\boldsymbol{\mu}$ is kept parallel

to the *z*-axis of the body-fixed frame in our simulations, which is only an approximation. A more realistic (though much more involved) treatment would consist in relaxing the previous constraint by fitting *ab-initio* calculations of each component of $\boldsymbol{\mu}$ by an analytical function. The APs would then be estimated from Eq. (24) with

$$cos\theta_{v\mu} = \frac{\mu_x v_x + \mu_y v_y + \mu_z v_z}{\mu v} \tag{28}$$

instead of Eq. (25). One expects that the distribution of $\theta_{v\mu}$ around $\pi/2$ would be broadened as compared with the previous treatment, thereby making the APs larger than $\sim$ -0.9. Nevertheless, Eq. (25) respects the fact that on average, the more excited the internal states of the diatoms, the larger the AP (see Fig. S5).

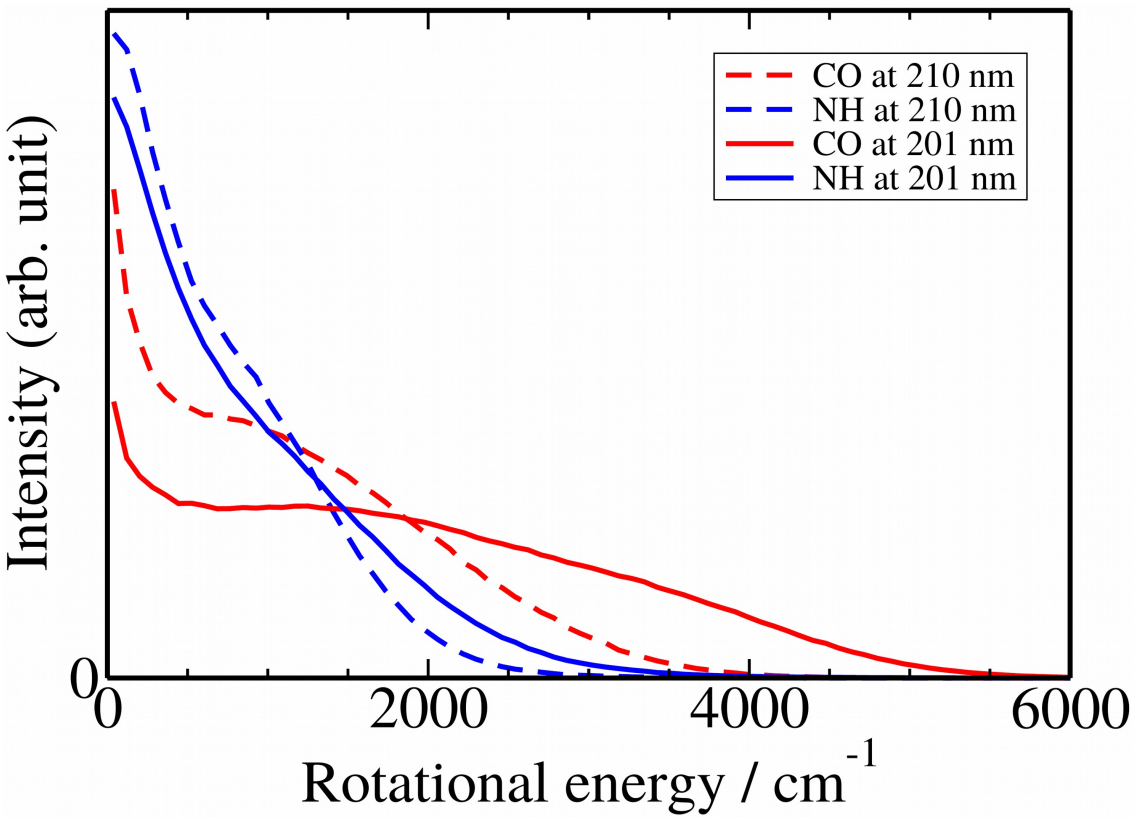

Fig. S 1: GB-CTM product rotational energy distributions. At both wavelengths, ^{1}NH is rotationally colder than CO.

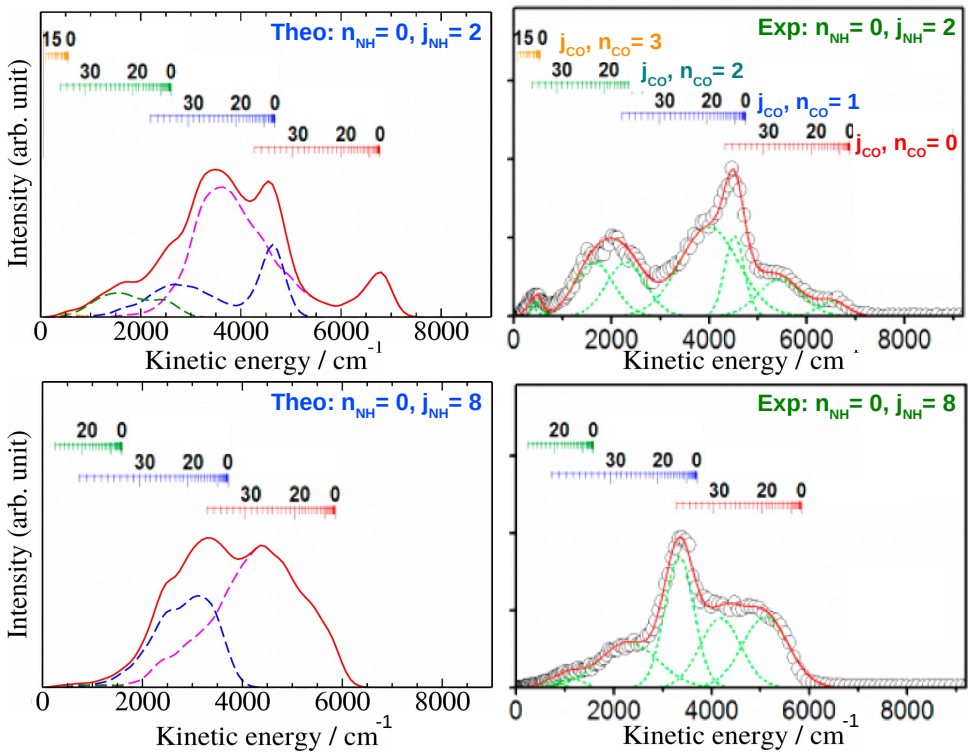

Fig. S 2: GB-CTM kinetic energy distributions at 201 nm for (n_{NH}, j_{NH}) =(0,2) and (0,8).

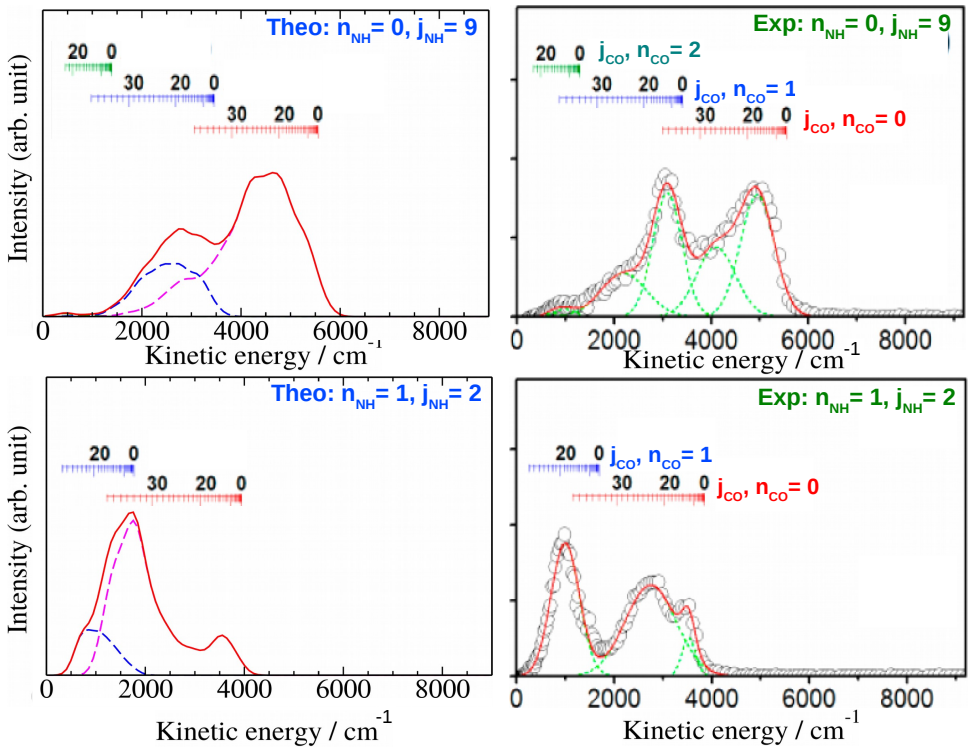

Fig. S 3: GB-CTM kinetic energy distributions at 201 nm for (n_{NH}, j_{NH}) =(0,9) and (1,2).

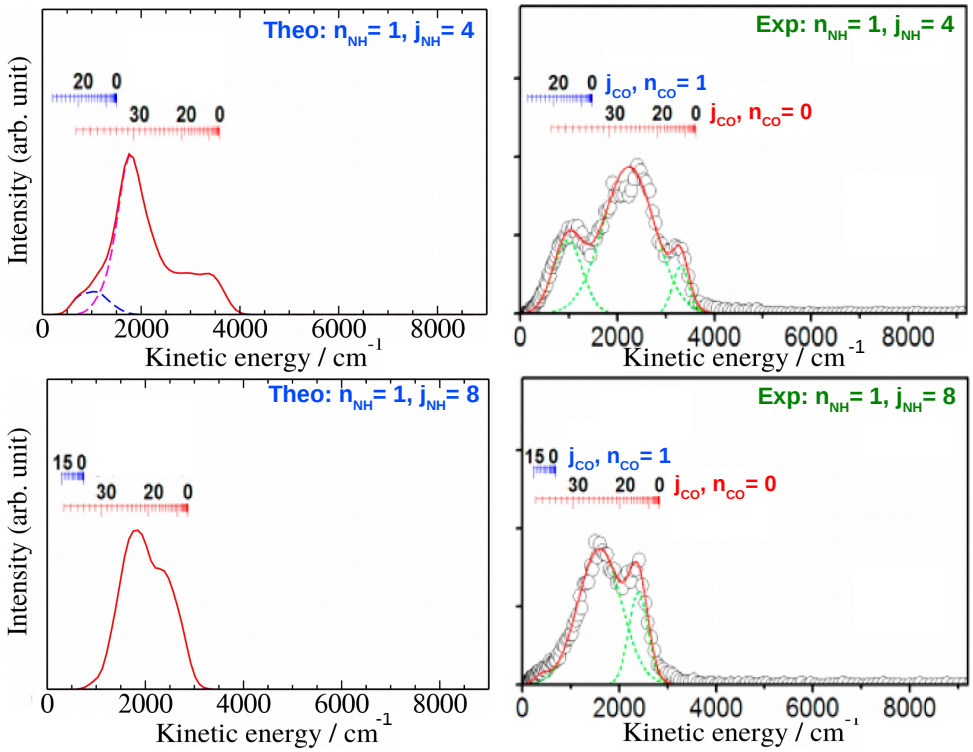

Fig. S 4: GB-CTM kinetic energy distributions at 201 nm for (n_{NH}, j_{NH}) =(1,4) and (1,8).

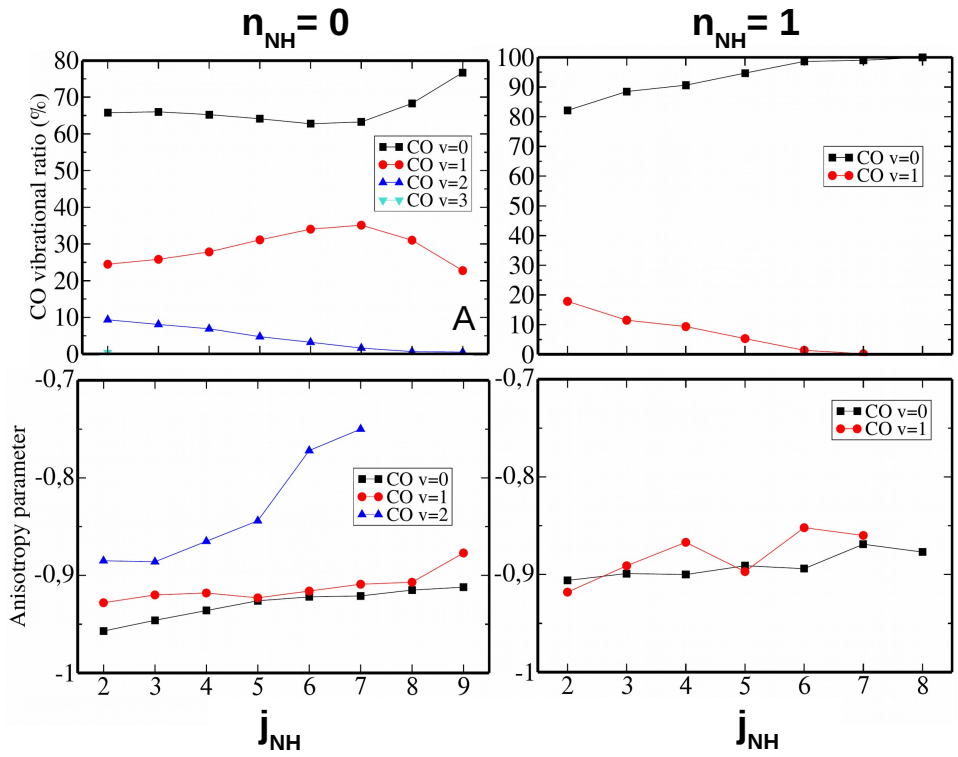

Fig. S 5: GB-CTM vibrational state distributions and anisotropy parameters at 201 nm.

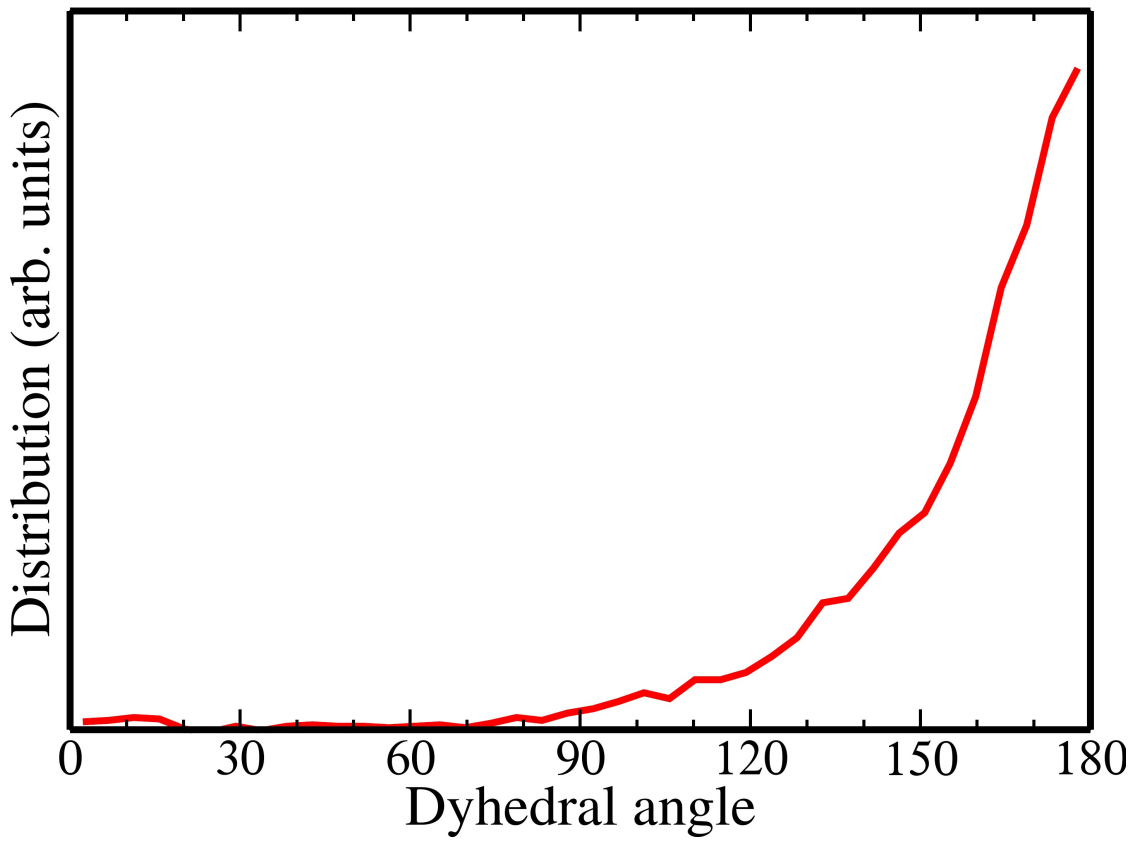

Fig. S 6: Distribution of the dihedral angle γ at the exit transition state at 201 nm.

References

(1) Klossika, J.-J.; Schinke, R. The Photodissociation of HNCO in the S_1 Band: A Five-Dimensional Classical Trajectory Study. *J. Chem. Phys.* **1999**, 111, 5882-5896.

(2) Korona, T.; Werner, H.-J. Local Treatment of Electron Excitations in the EOM-CCSD Method. *J. Chem. Phys.* **2003**, 118, 3006-3019.

(3) Hampel, C.; Peterson, K.; Werner, H.-J. A comparison of the Efficiency and Accuracy of the Quadratic Configuration Interaction (QCISD), Coupled Cluster (CCSD), and Brueckner Coupled Cluster (BCCD) Methods. *Chem. Phys. Lett.* **1992**, 190, 1-12.

(4) Dunning, Jr., T.H. Gaussian Basis Sets for Use in Correlated Molecular Calculations. I. The Atoms Boron Through Neon and Hydrogen. *J. Chem. Phys.* **1989**, 90, 1007-1023.

(5) Kendall, R. A.; Dunning, Jr., T. H.; Harrison, R. J. Electron Affinities of the First-Row Atoms Revisited. Systematic Basis Sets and Wave Functions. *J. Chem. Phys.* **1992**, 96, 6796-6806.

(6) MOLPRO is a package of *ab-initio* programs written by Werner, H.-J.; Knowles, P. J.; Knizia, G.; Manby, F. R.; Schütz, M.; Celani, P.; Györffy, W.; Kats, D.; Korona, T.; Lindh, R.; Mitrushenkov, A.; Rauhut, G.; Shamasundar, K. R.; Adler, T. B.; Amos, R. D.; Bernhardsson, A.; Berning, A.; Cooper, D. L.; Deegan, M. J. O.; Dobbyn, A. J.; Eckert, F.; Goll, E.; Hampel, C.; Hesselmann, A.; Hetzer, G.; Hrenar, T.; Jansen, G.; Köppl, C.; Liu, Y.; Lloyd, A. W.; Mata, R. A.; May, A. J.; McNicholas, S. J.; Meyer, W.; Mura, M. E.; Nicklaß, A.; O'Neill, D. P.; Palmieri, P.; Peng, D.; Pflüger, K.; Pitzer, R.; Reiher, M.; Shiozaki, T.; Stoll, H.; Stone, A. J.; Tarroni, R.; Thorsteinsson, T.; Wang, M.; see http://www.molpro.net.

(7) Wang, H.; Liu, S.-L.; Liu, J.; Wang, F.-Y.; Jiang, B.; Yang, X.-M. Photofragment Imaging of HNCO Decomposition at 210 nm: the Primary NH($a^1\Delta$)+CO($X^1\Sigma^+$) Channel. *Chinese J. Chem. Phys.* **2007**, 20, 388-394.

(8) Zhang, Z.; Chen, Z.; Huang, C.; Chen, Y.; Dai, D.; Parker, D. H.; Yang, X. Imaging the Pair-Correlated HNCO Photodissociation: The NH($a^1\Delta$) + CO($X^1\Sigma$) Channel. *J. Phys. Chem. A* **2014**, 118, 2413-2418.

(9) Schinke, R. Photodissociation Dynamics (Cambridge University Press, Cambridge, 1993).

(10) Goursaud, S.; Sizun, M.; Fiquet-Fayard, F. Energy Partitioning and Isotope Effects in the Fragmentation of Triatomic Negative Ions: Monte Carlo Scheme for a Classical Trajectory Study. *J. Chem. Phys.* **1976**, 65, 5453-5461.

(11) Press, W. H.; Teukolsky, S. A.; Vetterling, W. T.; Flannery, B. P. *Numerical Recipes in Fortran 90: The Art of Parallel Scientific Computing* (Cambridge University Press, Cambridge, 1997).

(12) Bonnet, L. Classical Dynamics of Chemical Reactions in a Quantum Spirit. *Int. Rev. Phys. Chem.* **2013**, 32, 171-228.

(13) Zare, R. N. *Angular Momentum* (John Wiley and Sons, New York, 1988). See Eq. (9), p. 121.

(14) Chang, Y.-T.; Minichino, C.; Miller, W. H. Classical Trajectory Studies of the Molecular Dissociation Dynamics of Formaldehyde: $H_2CO \rightarrow H_2$ + CO. *J. Chem. Phys.* **1992**, 96, 4341-4355.

(15) Houston, P. L.; Conte, R.; Bowman, J. M. Roaming Under the Microscope: Trajectory Study of Formaldehyde Dissociation. *J. Phys. Chem. A* **2016**, 120, 5103-5114.